



Revealing the coronal properties of Seyfert galaxies with NuSTAR

Andrea Marinucci (Roma Tre)

on behalf of the
NuSTAR AGN Physics WG

Florence
High Energy processes around compact objects
June 12, 2014

Overview

- Brief introduction on high-energy cutoff measurements
 - Nearby AGN seen by NuSTAR
 - Results
 - Conclusions and future perspectives

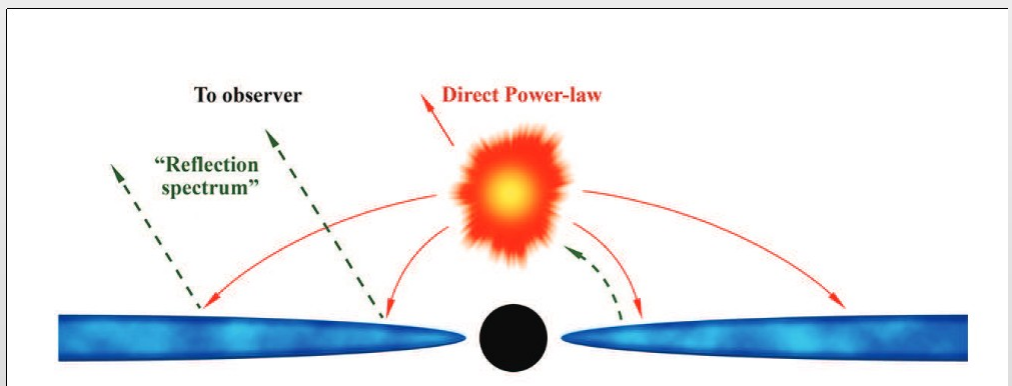
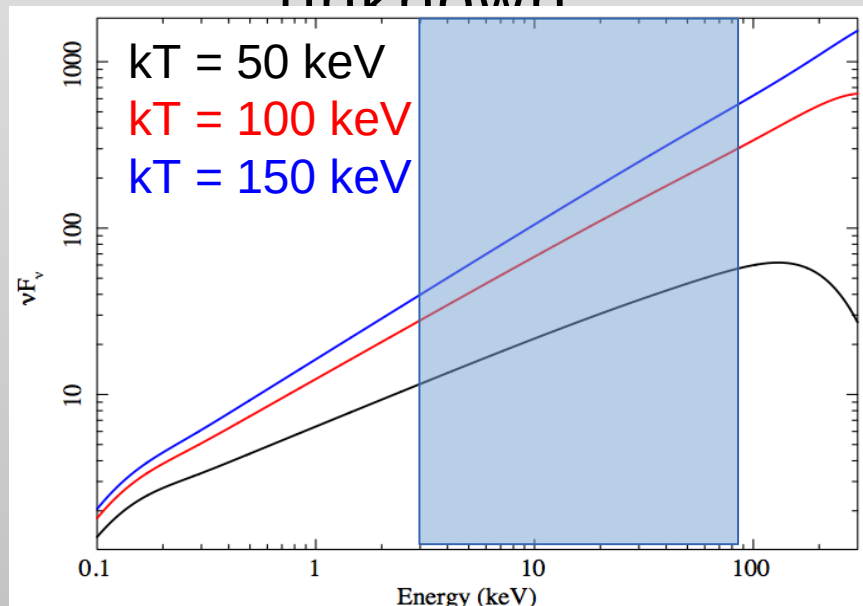
Overview

- Brief introduction on high-energy cutoff measurements
 - Nearby AGN seen by NuSTAR
 - Results
 - Conclusions and future perspectives

Introduction

One of the main open problem for AGN is the nature of the primary X-ray emission.

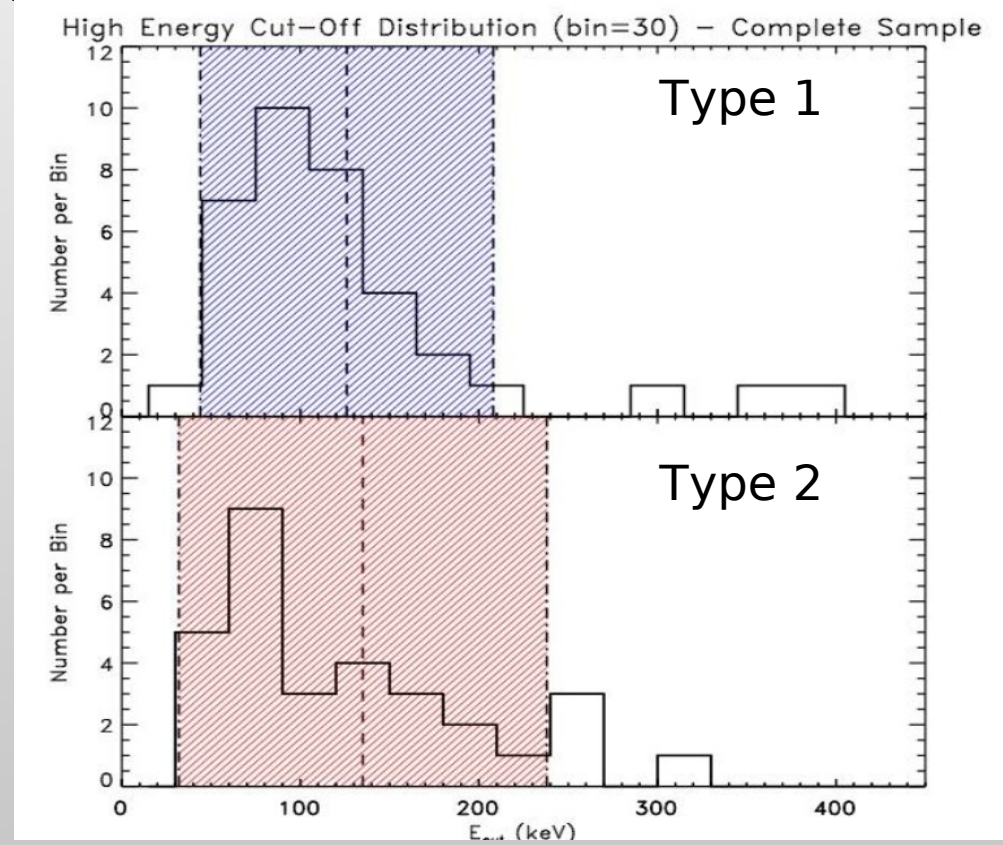
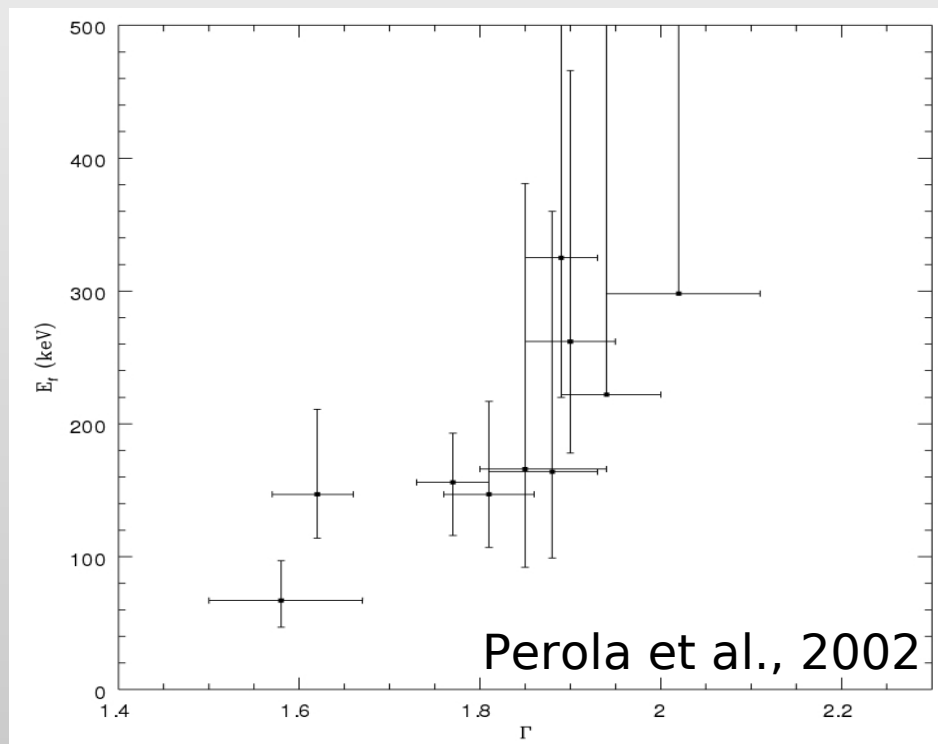
It is due to Comptonization of soft photons, but the geometry, optical depth and temperature of the emitting corona are largely unknown



Most popular models imply $E_{\text{cut}} = 2-3 \text{ kT}$, so measuring E_{cut} helps constraining Comptonization models.

Introduction

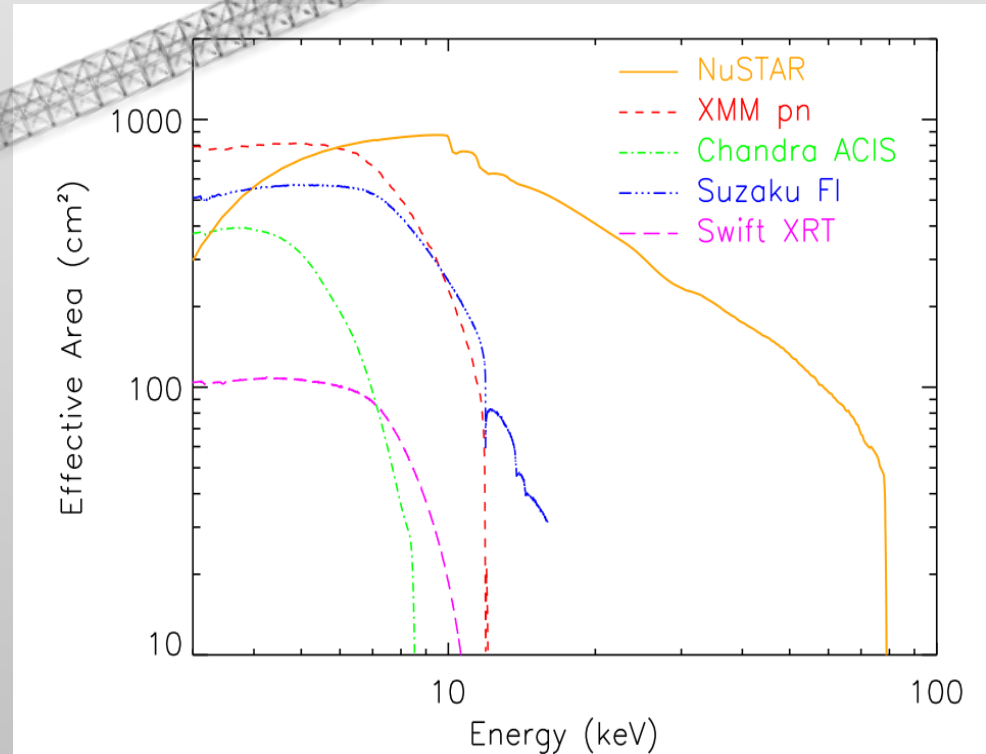
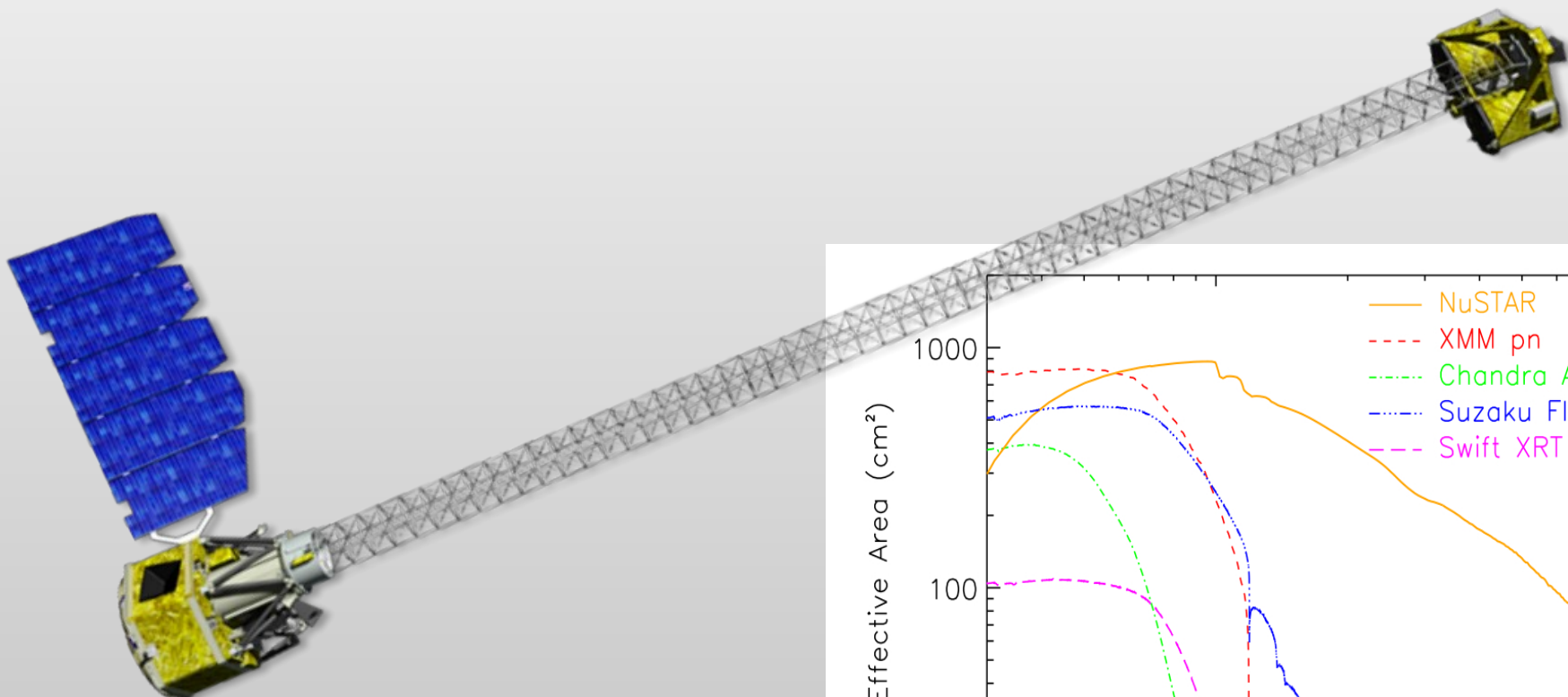
So far, we have only a handful of results based on non focusing, and therefore strongly background-dominated, satellites (BeppoSAX-PDS, Suzaku HXD-PIN, INTEGRAL, Swift-BAT)



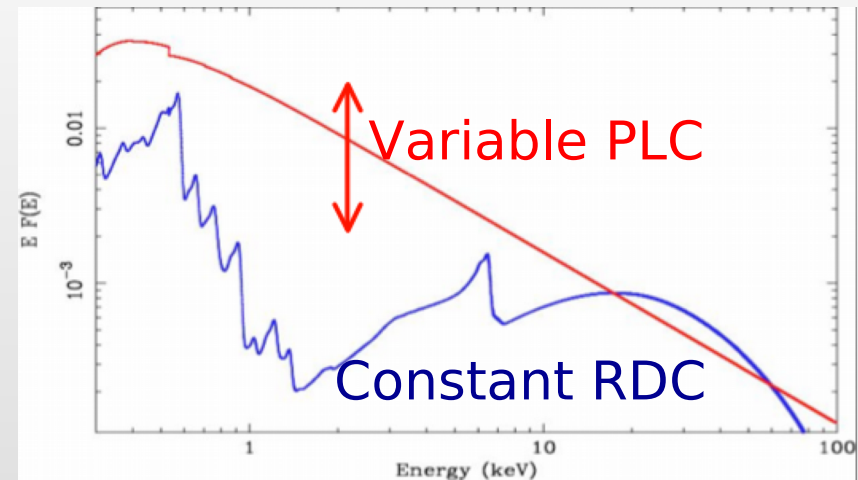
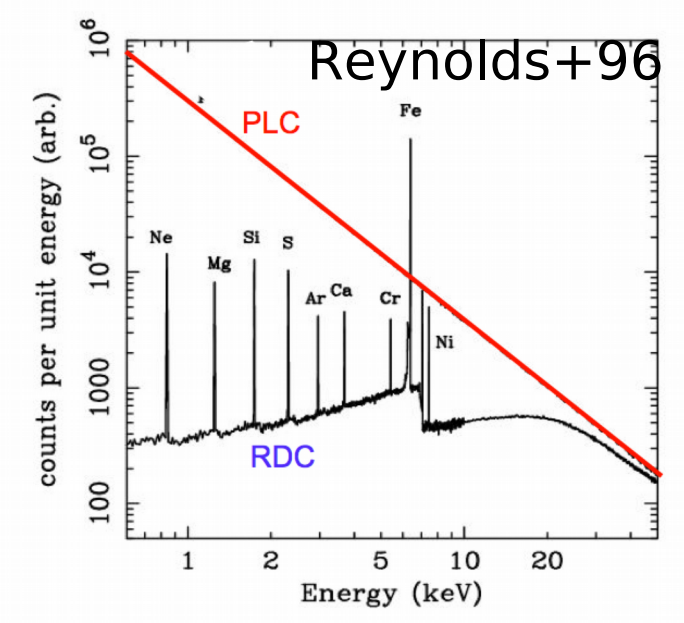
Overview

- Brief introduction on high-energy cutoff measurements
 - Nearby AGN seen by NuSTAR
 - Results
 - Conclusions and future perspectives

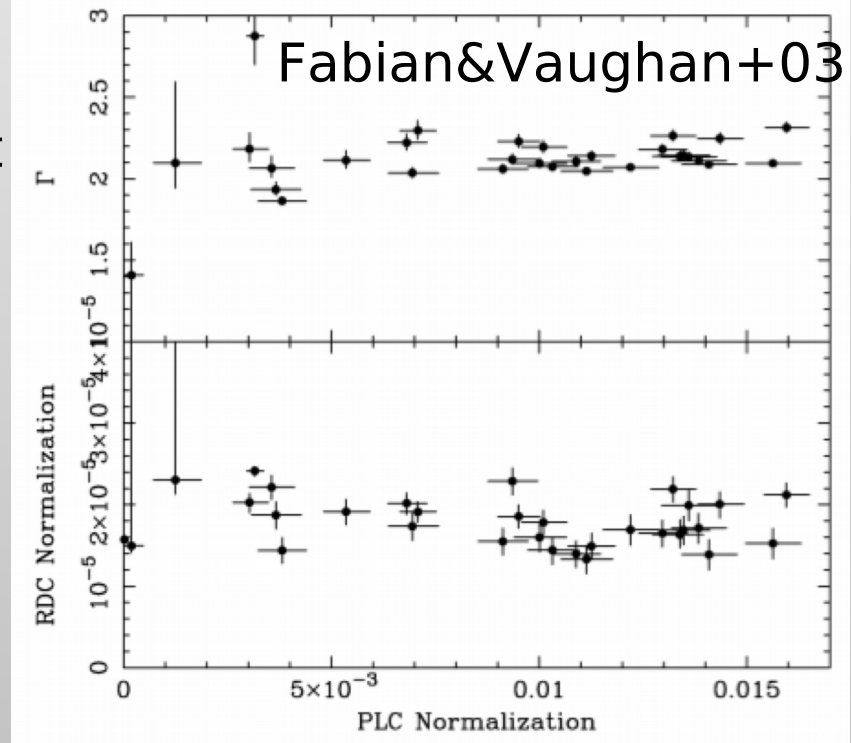
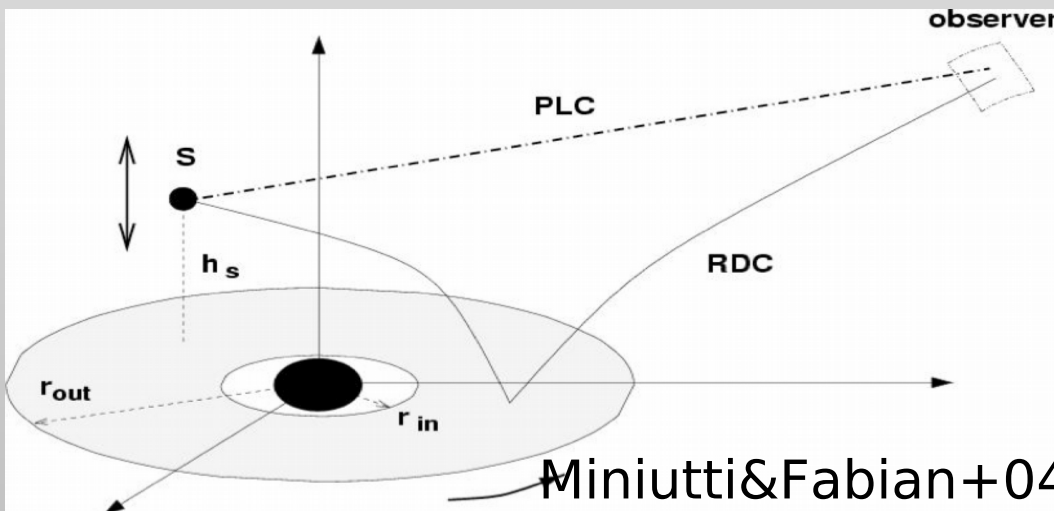
The NuSTAR satellite



Reflection scenario



Light bending model: much of the flux is bent onto the disk giving a constant, strong RDC



Absorption scenario

An alternative interpretation explains the spectral variability in terms of absorption changes

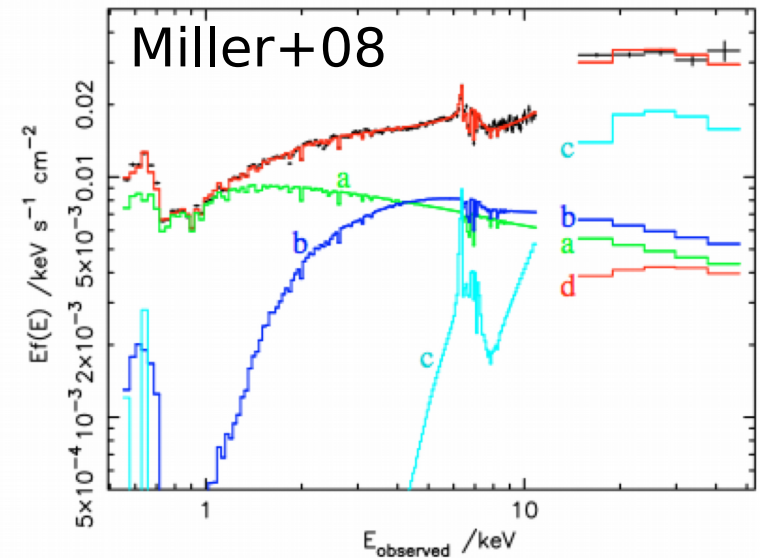
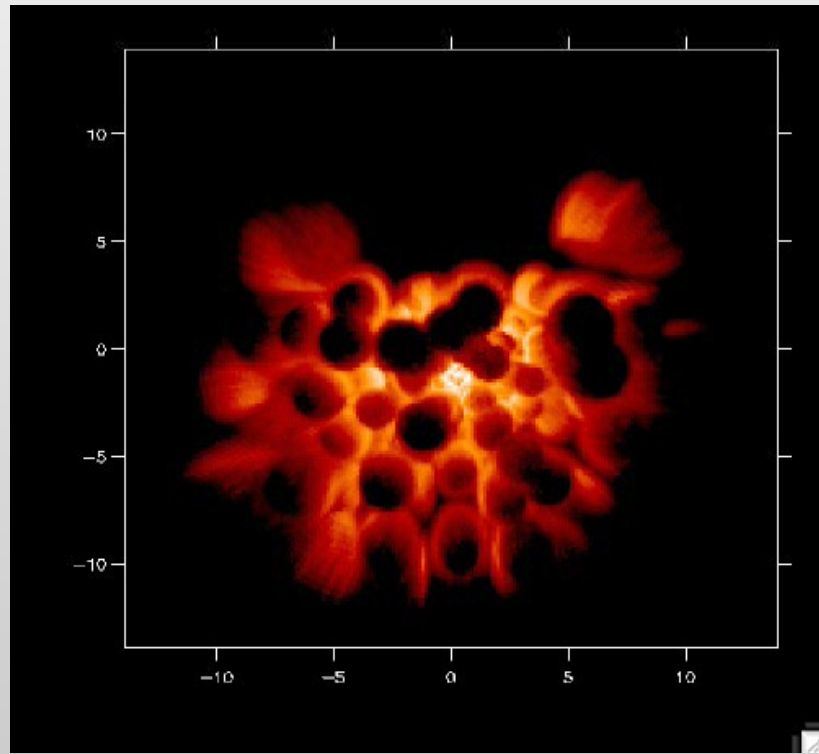


Fig. 4. Illustration of the spectral model. The upper curve shows the model fitted to the mean *Suzaku* spectrum, with XIS data below 11 keV and PIN data above 15 keV. Points with error bars show the unfolded data (see Sect. 4 for details). The three emission components are shown as (a) primary directly-viewed power-law, absorbed by zones 1 and 2; (b) fully covered power-law, absorbed by zones 1, 2, 3 and 5; (c) reflection, absorbed by zones 1, 2, 3 and 4. In the fit to the PCA components, zone 3 is excluded from eigenvector one; in the fit to the actual data, zone 3 is allowed to absorb all components. Also shown is the expected contribution of the cosmic X-ray background to the *Suzaku* PIN band (d) included in the model.

3 fully covering
warm absorbers

“3+2” MODEL

1 ionized absorber fully covering
the distant reflection component

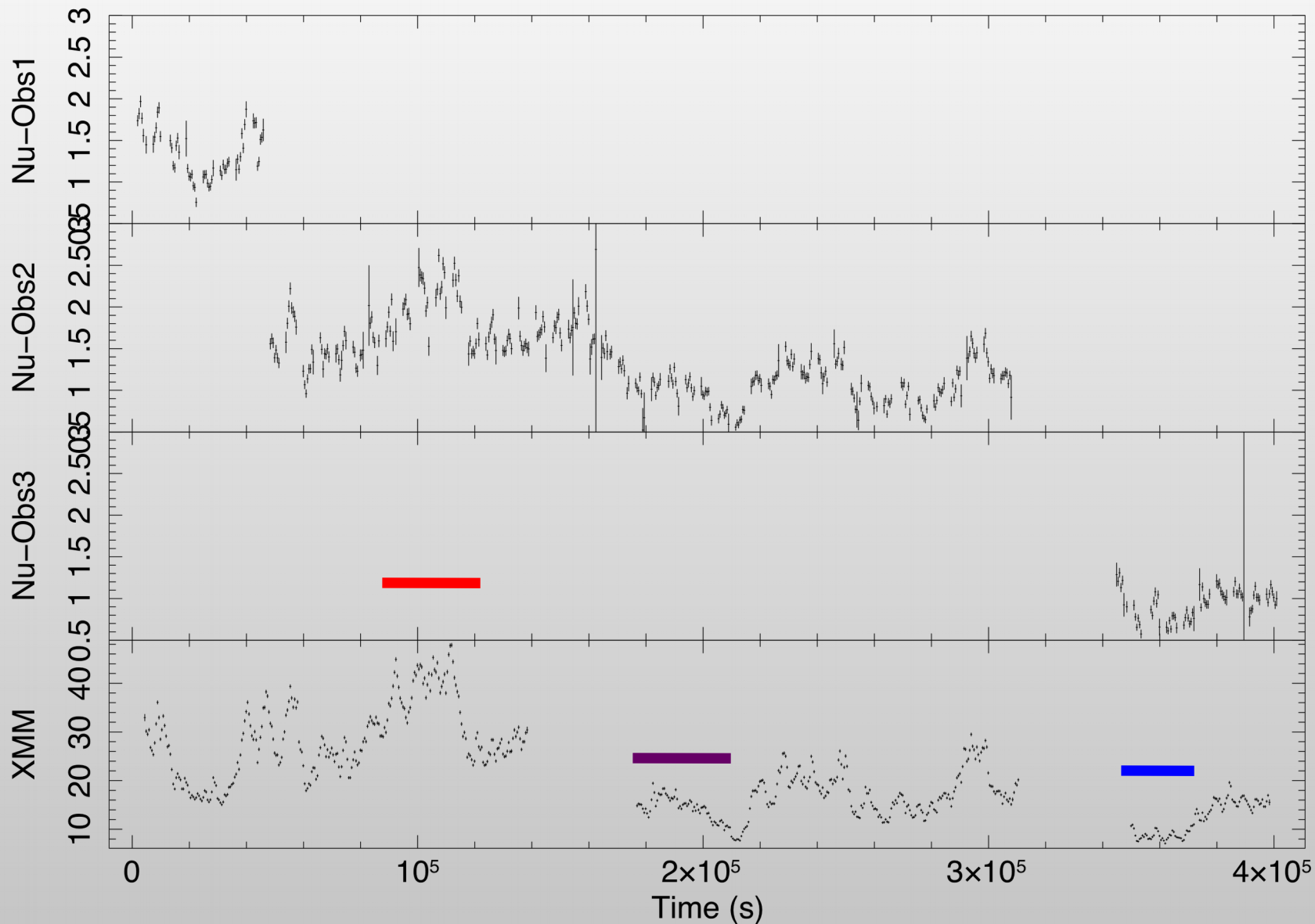
($N_H \sim 5 \times 10^{23} \text{ cm}^{-2}$, $\log \xi \sim 2.0$)

1 ionized absorber partial
covering the X-ray source
($N_H \sim 4 \times 10^{22} \text{ cm}^{-2}$, $\log \xi \sim 1.5$)

- Brief introduction on MCG-6-30-15
- The XMM-NuSTAR 2013 observational campaign
- Testing the two different scenarios
 - Results
- Conclusions and future perspectives

NuSTAR-XMM light curves

Bin time: 500.0 s

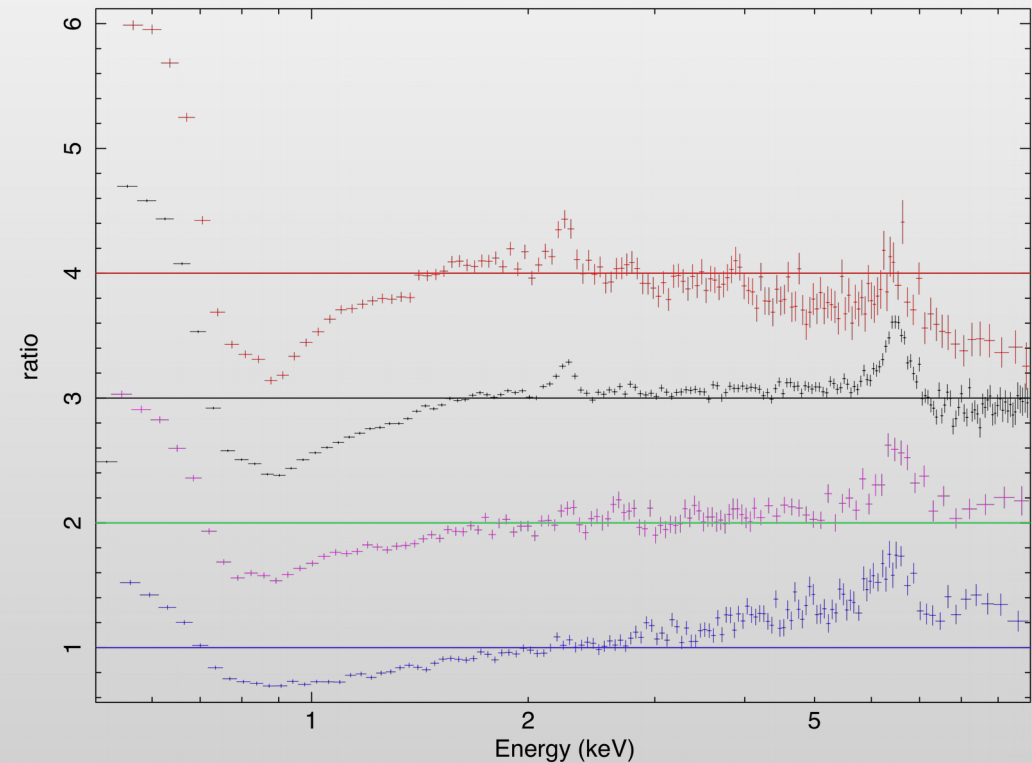


Start Time 16321 11:31:48:434 Stop Time 16326 2:21:48:434

Spectral features

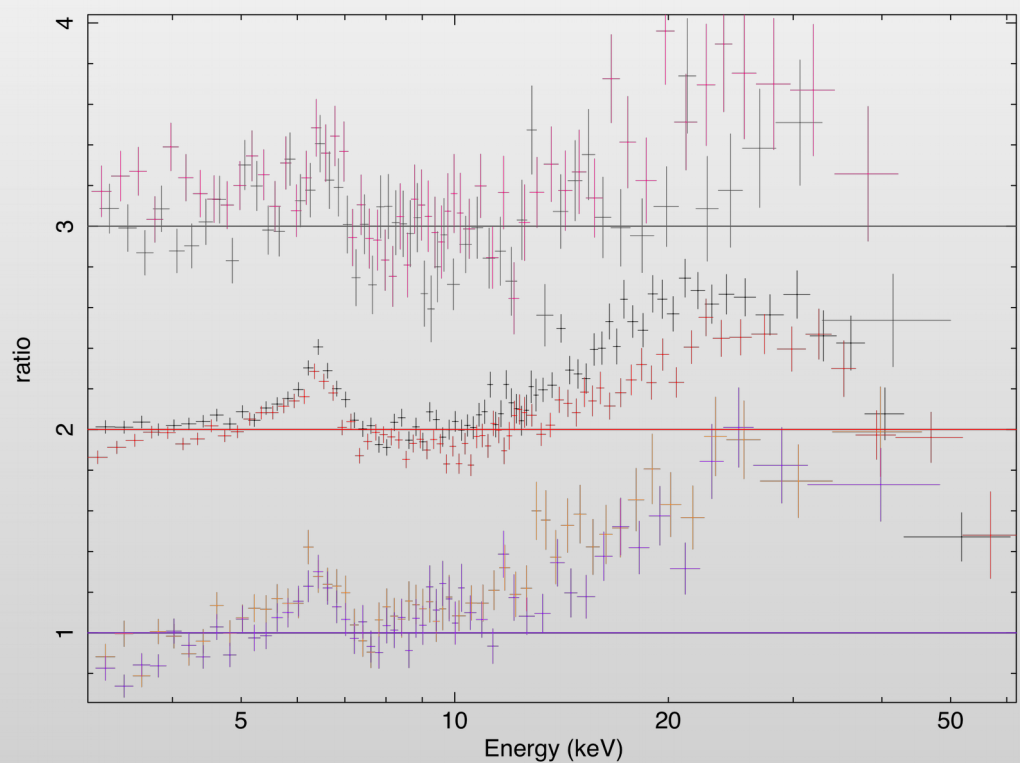
XMM-Newton EPIC-Pn

data/model



NuSTAR FpmA-FpmB

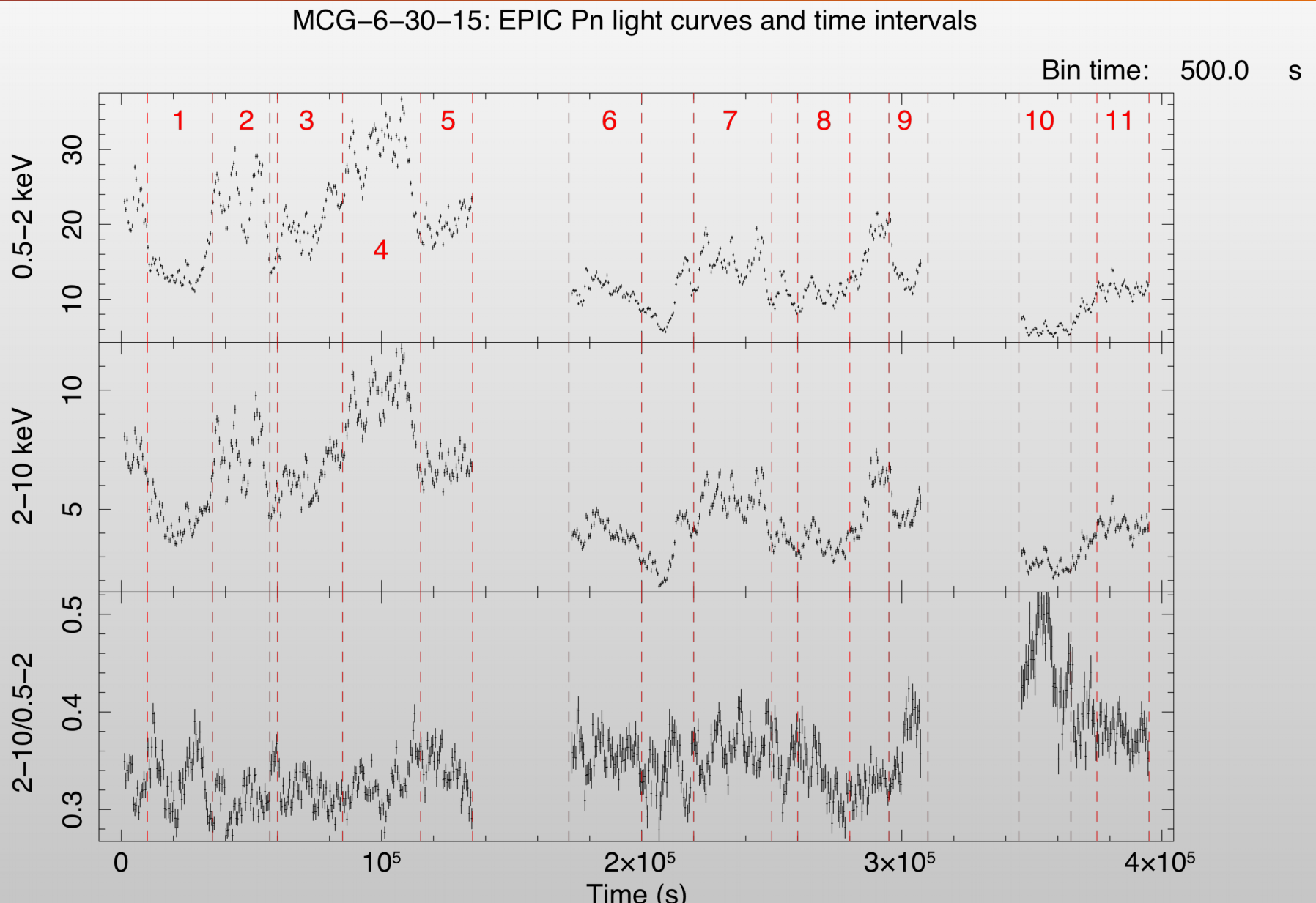
data/model



A broad Iron line, an intense soft excess and a strong Compton hump are present in the low flux spectrum (fit to a $\Gamma=2$ power law).

- Brief introduction on MCG-6-30-15
- The XMM-NuSTAR 2013 observational campaign
- Testing the two different scenarios
 - Results
- Conclusions and future perspectives

Fitting strategy



Start Time 16321 12:19:45:042 Stop Time 16326 1:38:05:042

Fitting strategy

Warm Absorbers

Combined RGS
spectra

Underlying Continuum

EPIC-Pn + NuSTAR
FpmA,B

REFLECTION

ABSORPTION

2*XSTAR*DUST

x

(Xillver + Relconv*Xillver + zpow)

2*XSTAR*DUST

x

(**XSTAR***Xillver + **XSTAR***zpo + zpo)

XSTAR tables

XILLVER instead of REFLIONX:

<http://hea-www.cfa.harvard.edu/~javier/xillver/>

Iron UTA tables for dust

RELCONV for relativistic blurring:

[http://www.sternwarte.uni-](http://www.sternwarte.uni-dortmund.de/~dowson/research/reflionx/)

[dortmund.de/~dowson/research/reflionx/](http://www.sternwarte.uni-dortmund.de/~dowson/research/reflionx/)

Combined RGS1+2 analysis

$$N_{H1} = (4.6 \pm 0.8) \times 10^{20} \text{ cm}^{-2}$$

$$\log \xi_1 = 1.47 \pm 0.2$$

$$v \sim 2000 \text{ km s}^{-1}$$

$$N_{H2} = (1.3 \pm 0.2) \times 10^{20} \text{ cm}^{-2}$$

$$\log \xi_2 = 0.08 \pm 0.10$$

$$N_{H3} = (1.00 \pm 0.04) \times 10^{22} \text{ cm}^{-2}$$

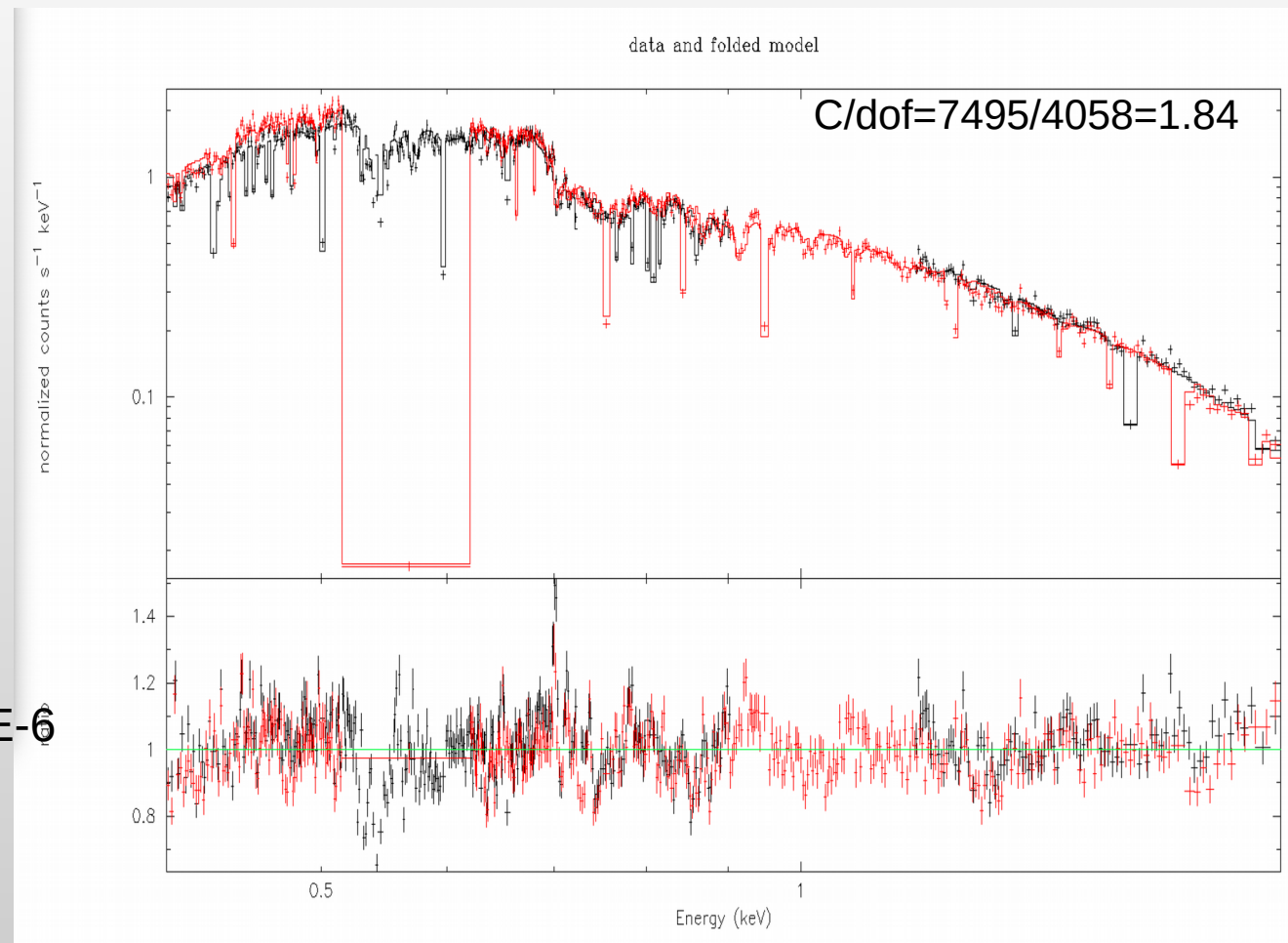
$$\log \xi_3 = 2.03 \pm 0.01$$

$$\log N_{Fe} = 17.32 \pm 0.02$$

xillver Norm = $9.3E-06 \pm 0.8E-6$

$$\Gamma = 2.03 \pm 0.02$$

$$\text{norm } 1.58E-02 \pm 0.02E-2$$



We then applied the combined best fit to the three separate RGS1+2 data sets

Separate RGS1+2 analysis

Orbit 1

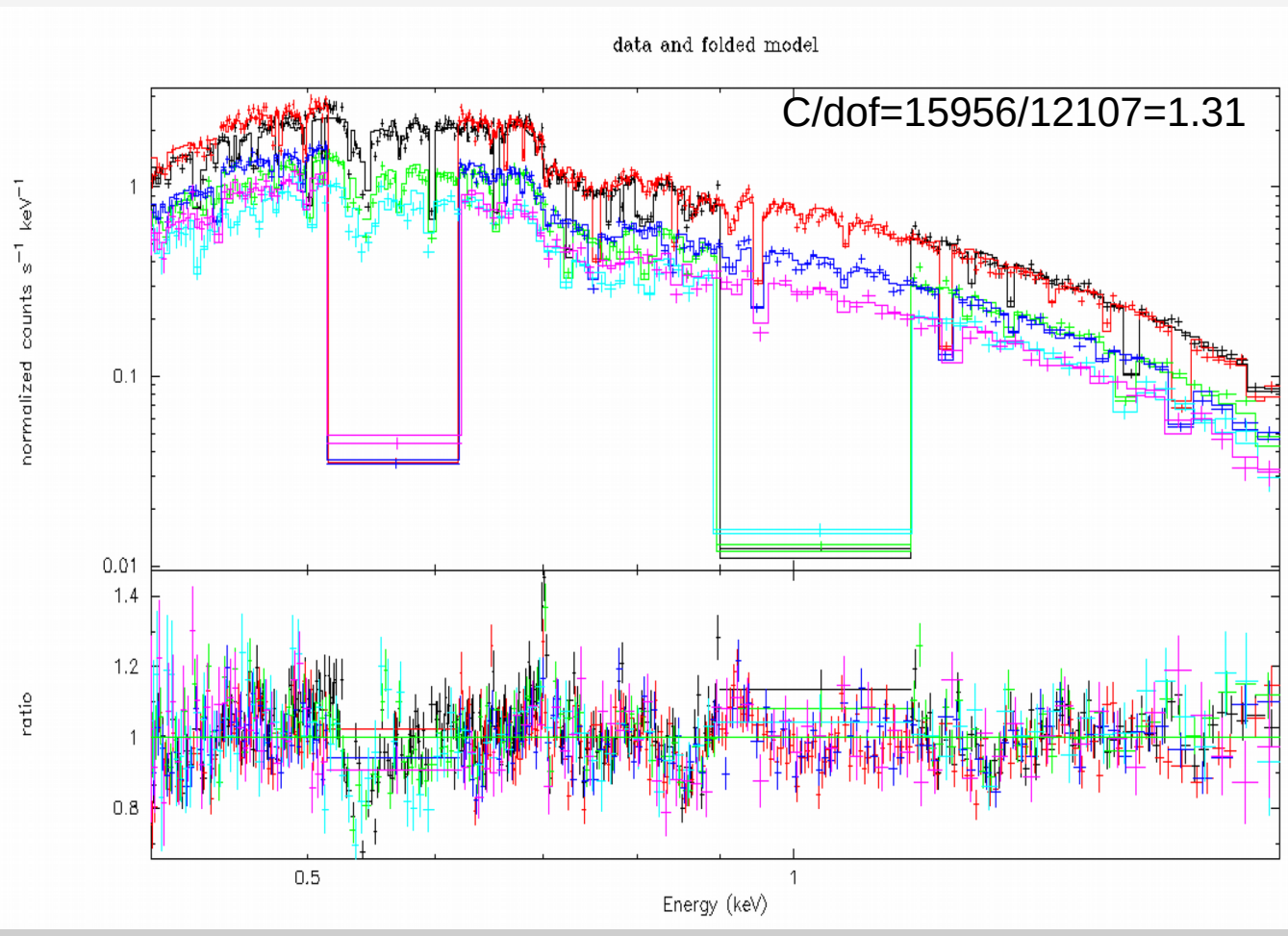
$N_{H_1} (5.6 \pm 1.7) \times 10^{20} \text{ cm}^{-2}$
 $\log \xi_1 1.82 \pm 0.05$
 $v \sim 2000 \text{ km s}^{-1}$
 $N_{H_2} (8.6 \pm 1.8) \times 10^{20} \text{ cm}^{-2}$
 $\log \xi_2 1.47 \pm 0.05$
 $N_{H_3} (1.00 \pm 0.04) \times 10^{22} \text{ cm}^{-2}$
 $\log \xi_3 2.04 \pm 0.01$
 $\log N_{Fe} 17.33 \pm 0.02$

 xillver norm $9.3E-06 \pm 0.8E-06$
 $\Gamma = 2.03^*$
 norm $1.58E-02 \pm 0.02E-2$

Orbit 2

$N_{H_1} (4.0 \pm 1.8) \times 10^{20} \text{ cm}^{-2}$
 $\log \xi_1 1.85 \pm 0.1$
 $v \sim 2000 \text{ km s}^{-1}$
 $N_{H_2} (2.9 \pm 0.5) \times 10^{20} \text{ cm}^{-2}$
 $\log \xi_2 1.34 \pm 0.13$
 $N_{H_3} (1.00 \pm 0.09) \times 10^{22} \text{ cm}^{-2}$
 $\log \xi_3 2.02 \pm 0.02$
 $\log N_{Fe} 17.27 \pm 0.04$
 $\Gamma = 2.03$
 norm $1.22E-02 \pm 0.02E-02$

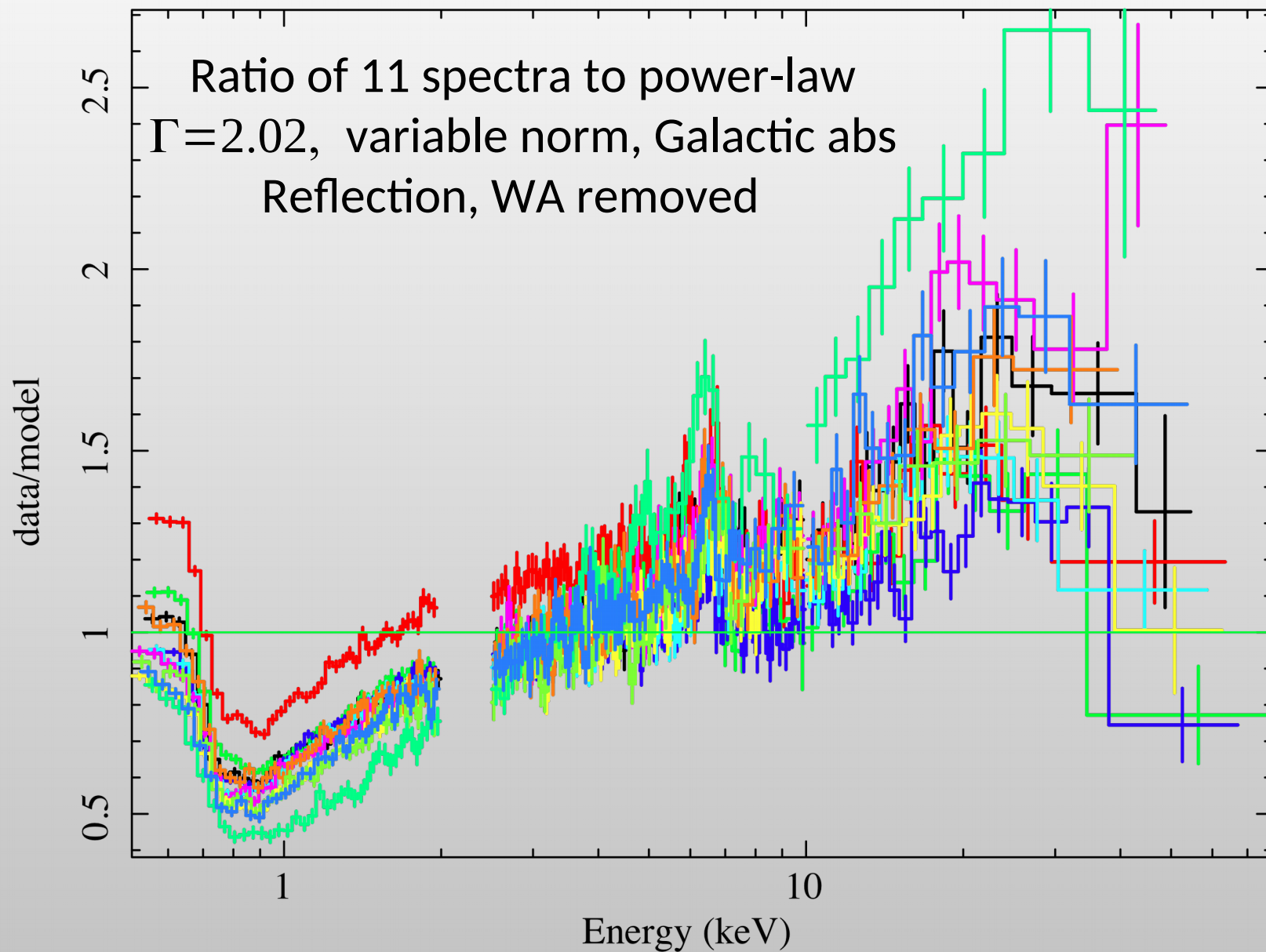
No significant variation has been found in the warm absorbing structure



Orbit 3

$N_{H_1} (5.1 \pm 2.5) \times 10^{20} \text{ cm}^{-2}$ $\log \xi_1 1.75 \pm 0.23$ $v \sim 2000 \text{ km s}^{-1}$ $N_{H_2} (5.0 \pm 1.0) \times 10^{20} \text{ cm}^{-2}$ $\log \xi_2 1.3 \pm 0.3$	$N_{H_3} (0.88 \pm 0.02) \times 10^{22} \text{ cm}^{-2}$ $\log \xi_3 2.00 \pm 0.03$ $\log N_{Fe} 17.08 \pm 0.12$ $\Gamma = 2.03$ norm $0.8E-02 \pm 0.4E-03$
---	---

Time resolved simultaneous analysis



- Brief introduction on MCG-6-30-15
- The XMM-NuSTAR 2013 observational campaign
- Testing the two different scenarios
 - **Results**
- Conclusions and future perspectives

Results: reflection

Warm absorbers

$$N_{H1} = (0.6\text{--}2.5) \times 10^{22} \text{ cm}^{-2}$$

$$\log \xi_1 = 1.98 \pm 0.01$$

$$N_{H2} = (0.5\text{--}3.0) \times 10^{21} \text{ cm}^{-2}$$

$$\log \xi_2 = 1.27 \pm 0.02$$

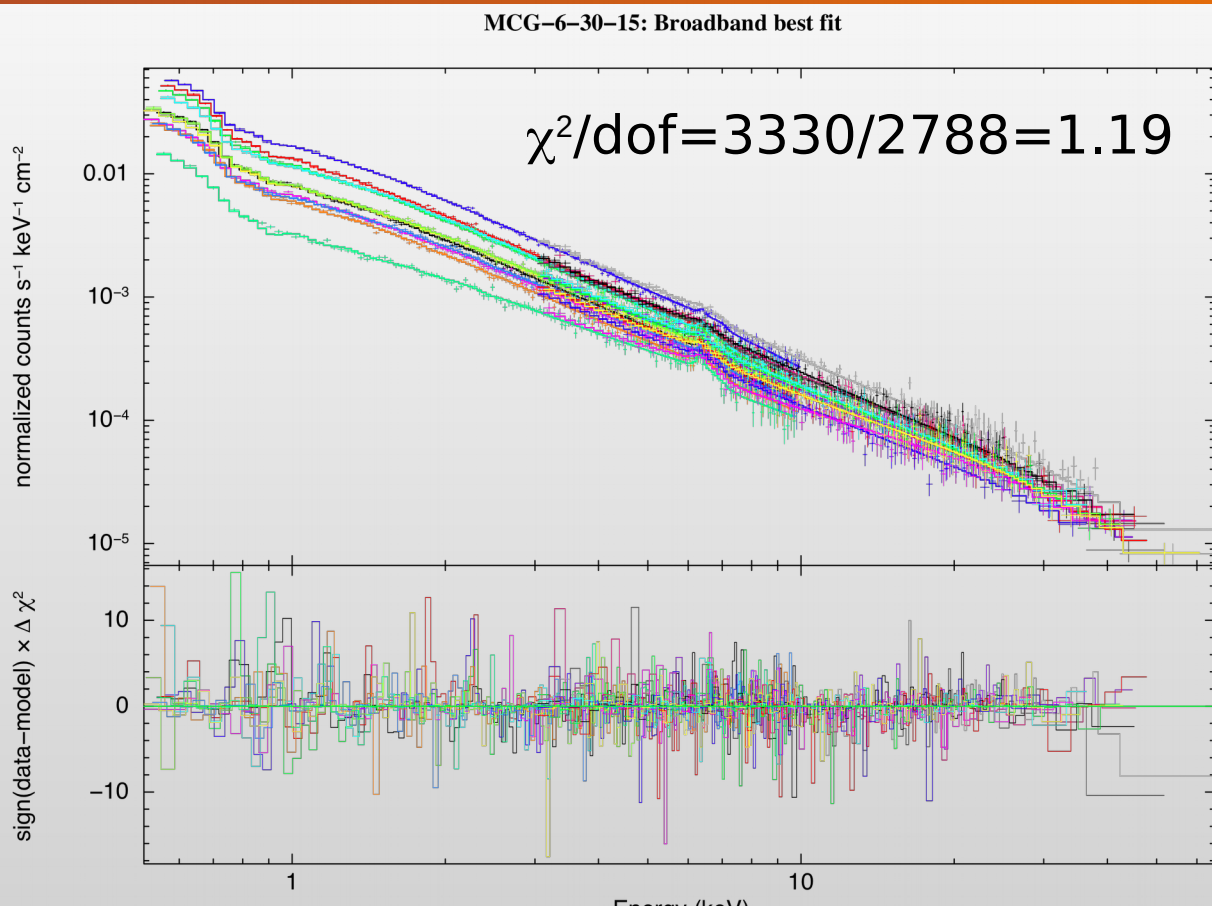
$$\log N_{Fe} = 16.6 \pm 0.2$$

Reflection parameters

$$(q=3.0 \text{ } a=0.998 \text{ } incl=37^\circ)$$

$$\log \xi = 0.2\text{--}3.0$$

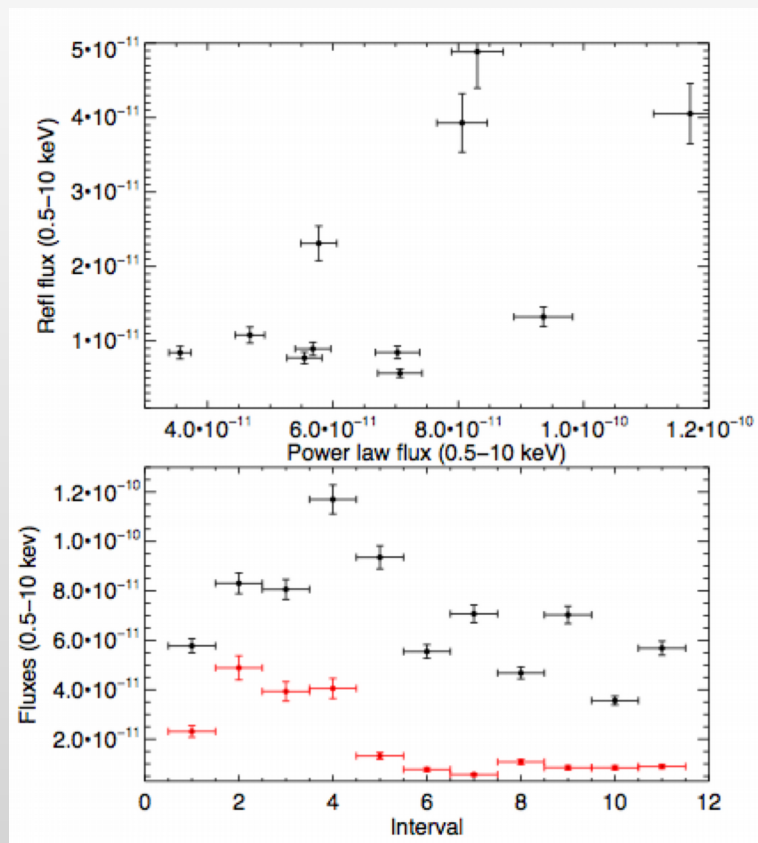
$$A_{Fe} = 1.56 \pm 0.32$$



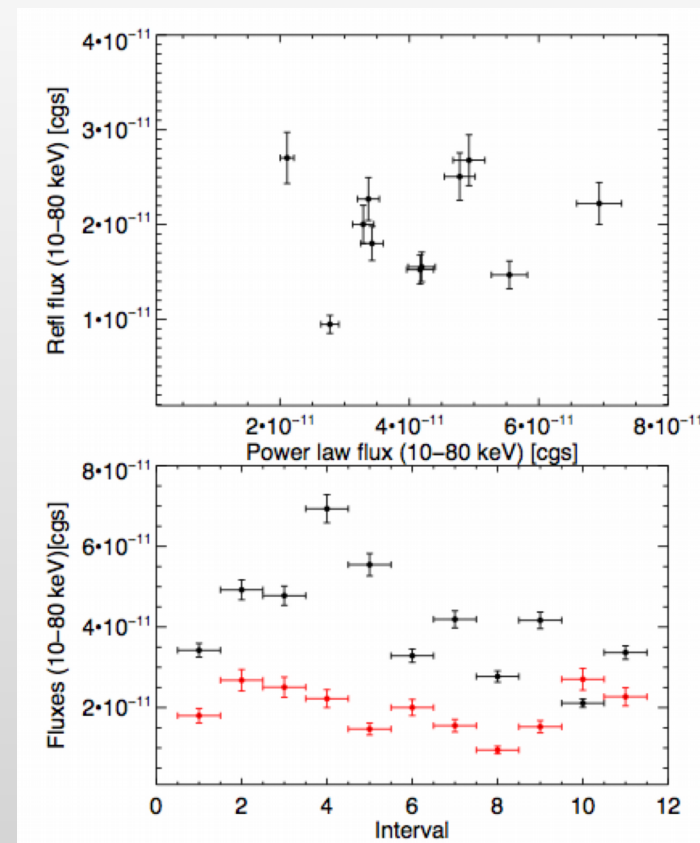
Primary emission parameters

$$\Gamma = 2.050 \pm 0.005$$
$$E_c > 100 \text{ keV}$$

RDC vs PLC fluxes



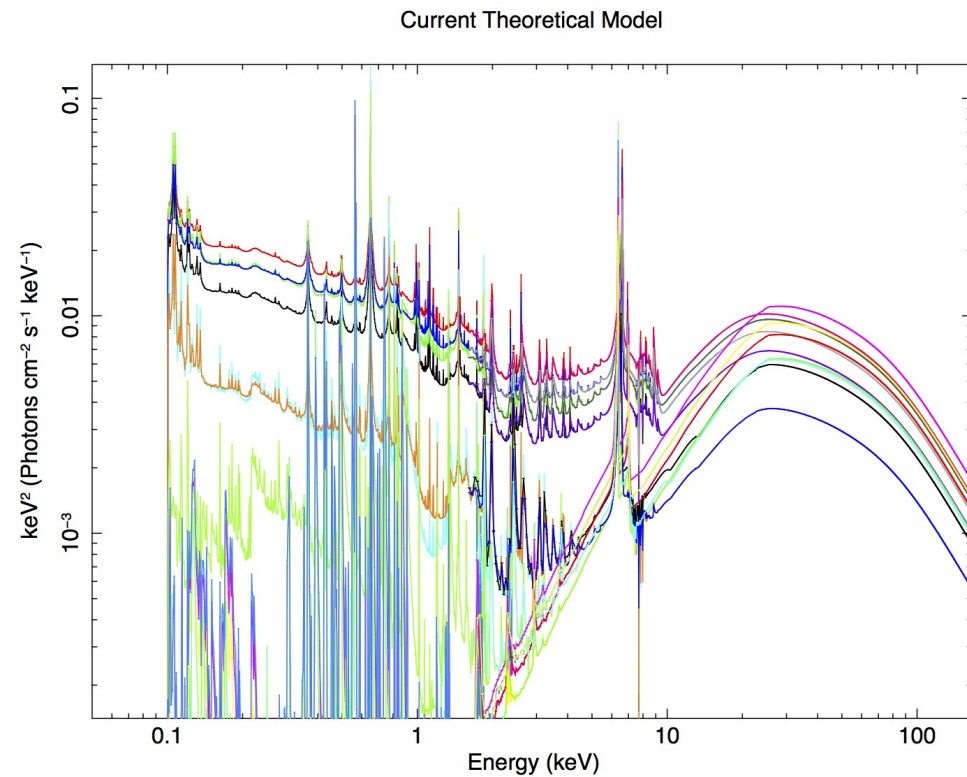
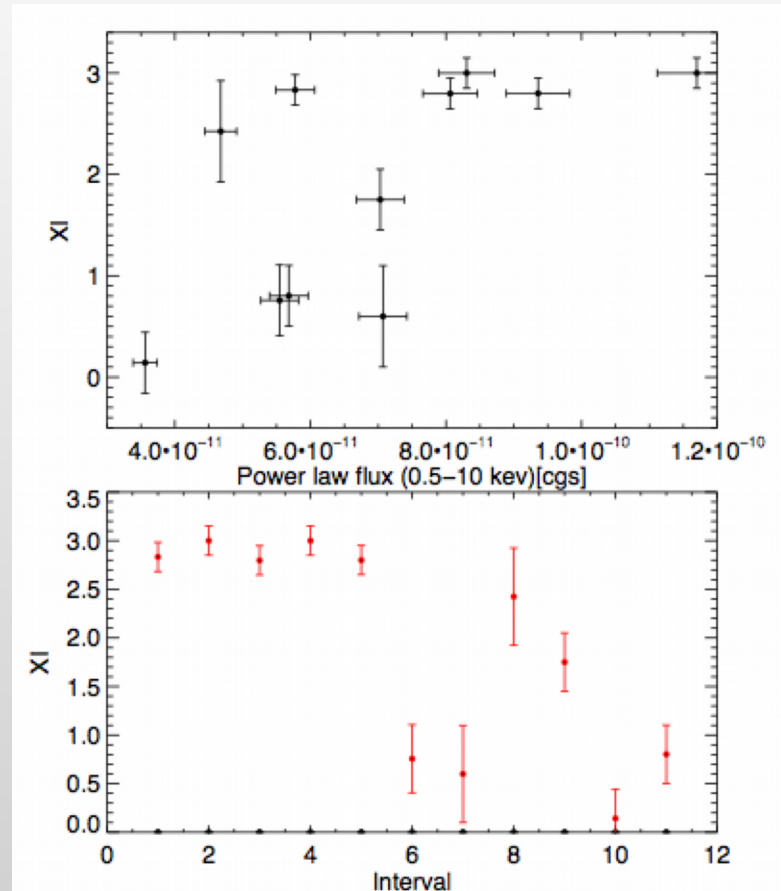
Variation of a factor ~ 2 observed in the RDC between 0.5-10 keV, in agreement with the PCA (Parker et al., submitted)



Constancy of the RDC between 10-80 keV (thanks to NuSTAR)

Marginal response from the accretion disk to the nuclear emission?

Accretion disk response



There is a response of the ionization state of the accretion disk to the variation of the PLC

Results: absorption

2 warm absorbers

$$N_{H1} = (1.3 \pm 0.2) \times 10^{22} \text{ cm}^{-2}$$

$$\log \xi_1 = 1.95 \pm 0.02$$

$$N_{H2} = (4.2 \pm 1.5) \times 10^{21} \text{ cm}^{-2}$$

$$\log \xi_2 = 2.82 \pm 0.05$$

$$\log N_{Fe} = 16.9 \pm 0.1$$

Further absorbers

(Xillver: $\log \xi = 2.4 \pm 0.05$;
 $A_{fe} = 0.5 \pm 0.1_p$)



$$N_{H3} = (3.0 \pm 0.4) \times 10^{23} \text{ cm}^{-2}$$

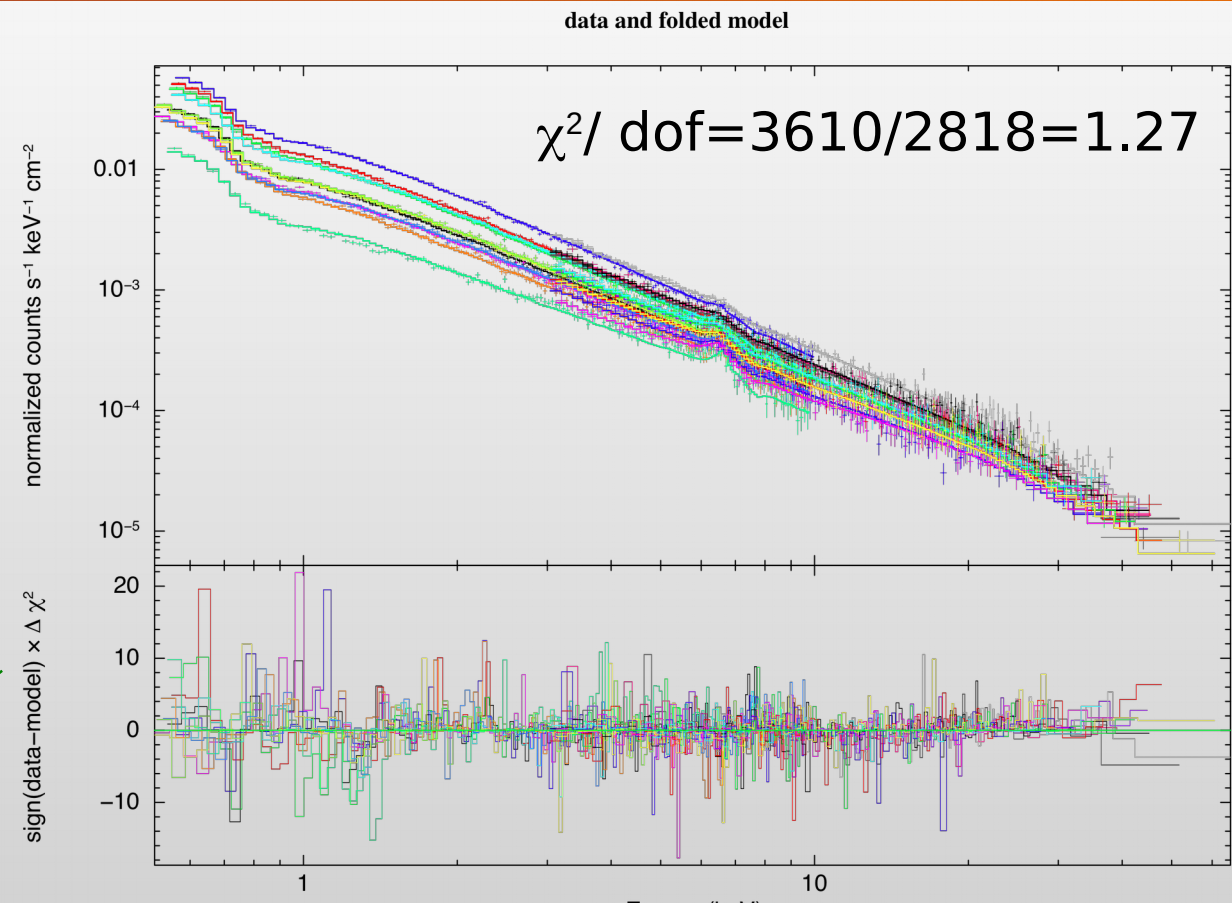
$$\log \xi_3 = 2.11 \pm 0.01$$



$$N_{H4} = (0.3-27) \times 10^{21} \text{ cm}^{-2}$$

$$\log \xi_4 = (0.0015 \pm 0.0005)$$

[almost neutral]

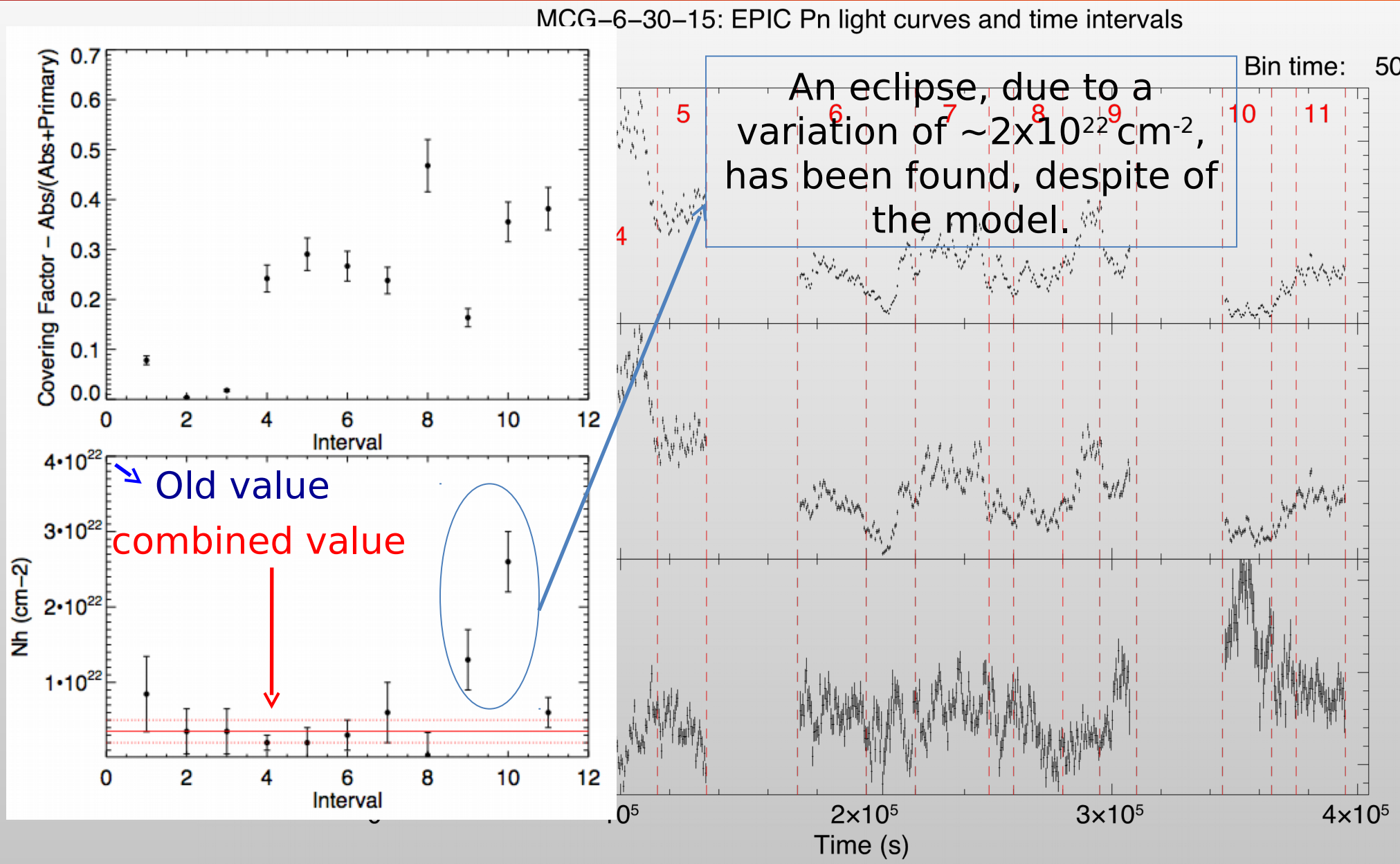


Primary emission parameters

$$\Gamma = 2.16 \pm 0.01$$

$$E_c > 100 \text{ keV}$$

Covering factor time evolution



- Brief introduction on MCG-6-30-15
- The XMM-NuSTAR 2013 observational campaign
- Testing the two different scenarios
 - Results
- Conclusions and future perspectives

Conclusions

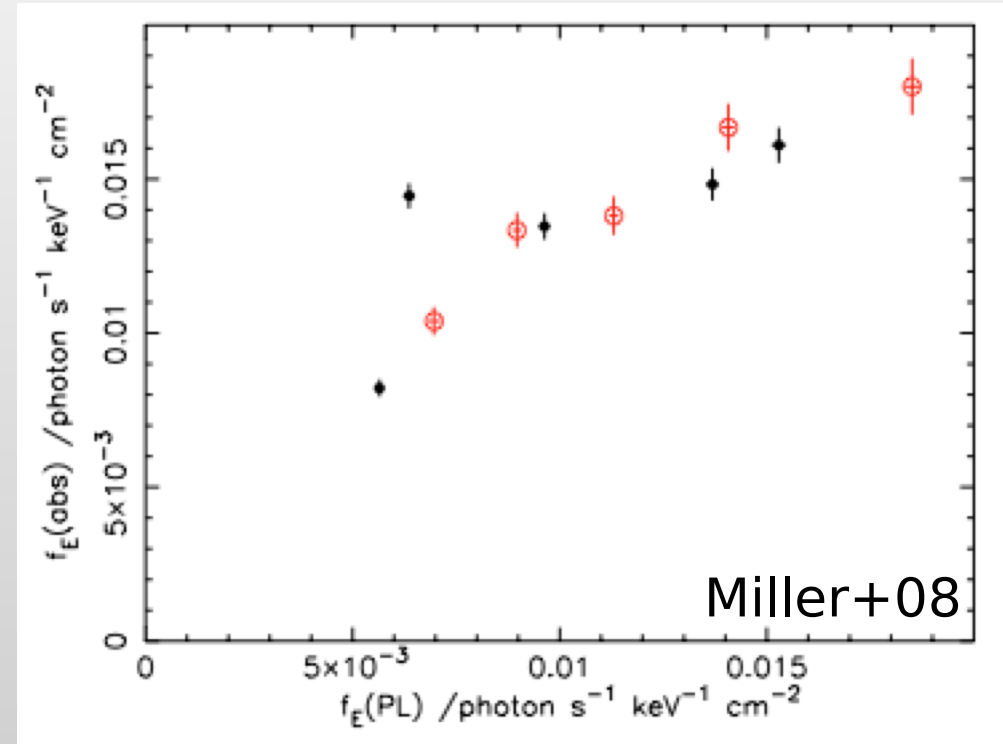
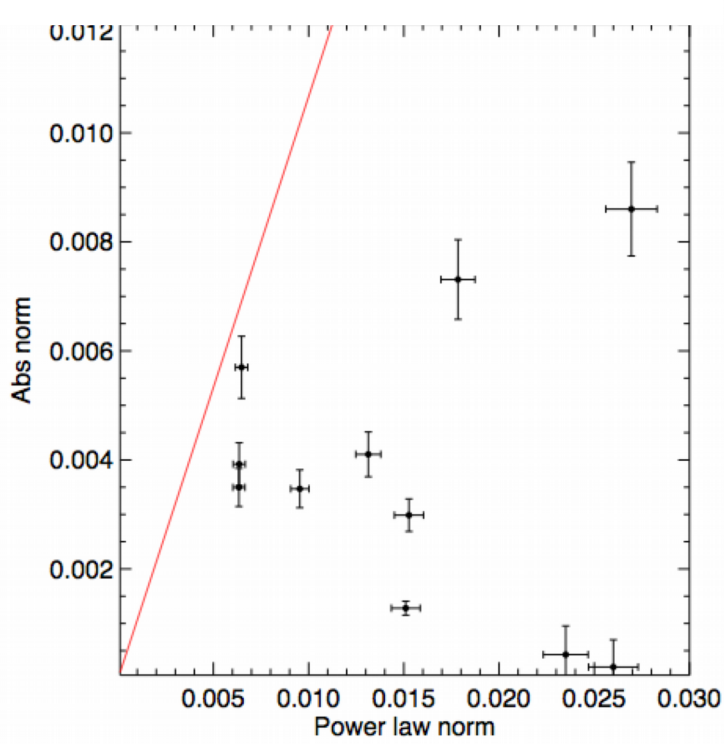
- The warm absorbing structure is consistent with literature, except for the lack of highly ionized absorption lines;
- The reflection scenario well explains the behavior of the source, from **0.4 keV** up to **80 keV** and it is statistically preferred
- Spectral variability can be explained in terms of strong variations of the PLC and to marginal variations in the RDC
- An alternative is that the spectral variability can be attributed to a change in covering fraction of the X-ray source AND to a change of N_H .

Future perspectives

- Explore the parameter space with greater detail (leaving other parameters free to vary);
- Increase the S/N: spectra with longer exposure times should, in principle, allow us to discriminate between a model with $\Gamma=2.05$ and $\Gamma=2.15$;
- Time intervals with constant HR **AND** comparable flux (in a fixed energy band) could be co-added.
- Measure cut-off energy (so far only a lower limit of 100 keV has been inferred)
- Measure Black Hole spin throughout the 300 ks observation

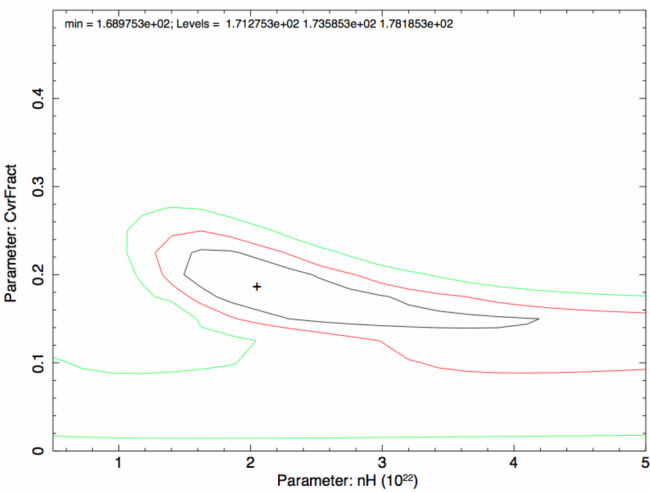


Backup

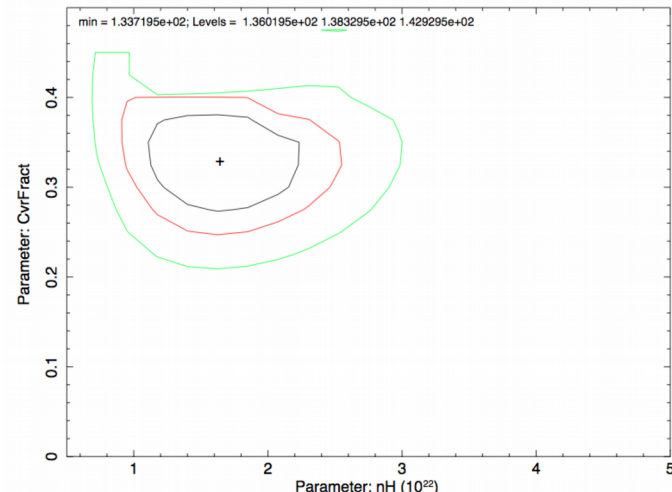


Backup

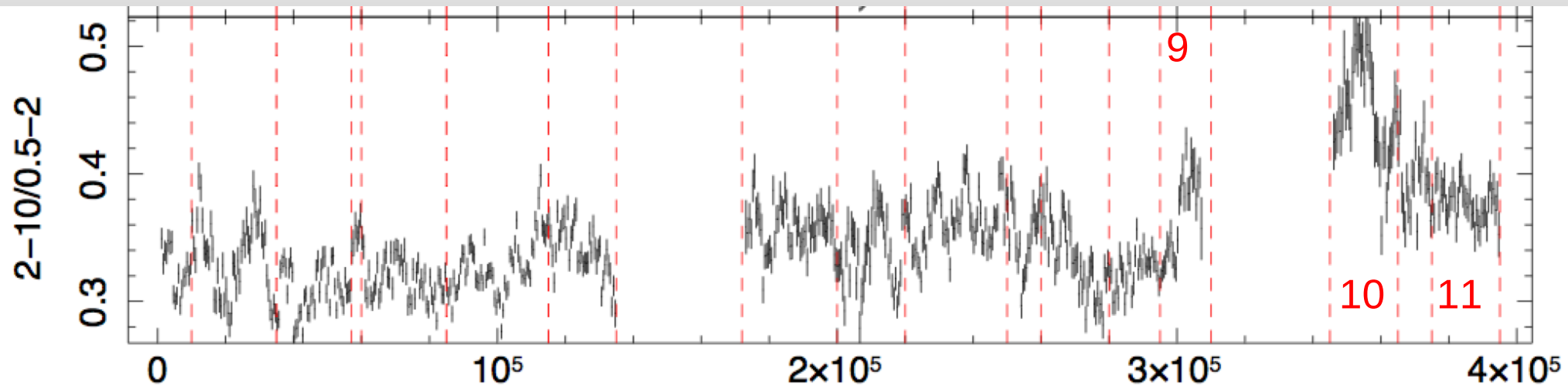
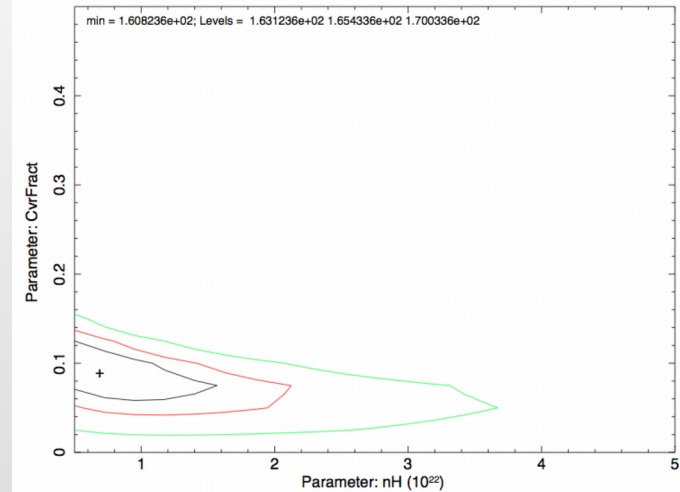
Confidence contours: INTERVAL 9



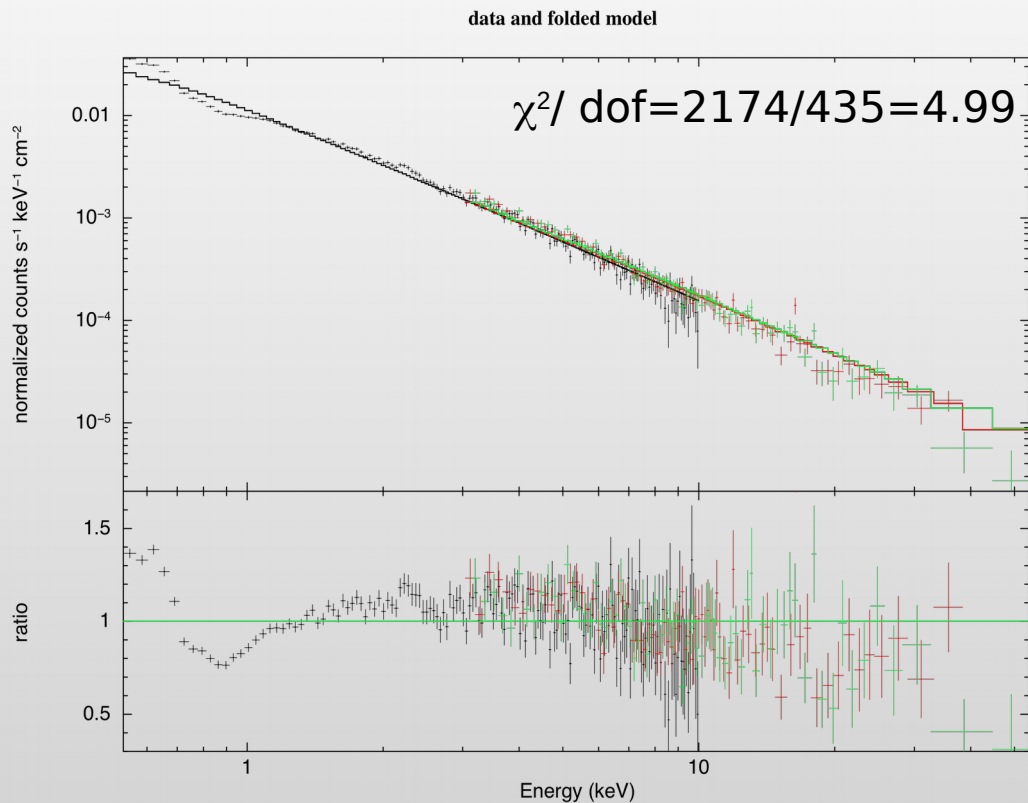
Confidence contours: INTERVAL 10



Confidence contours: INTERVAL 11

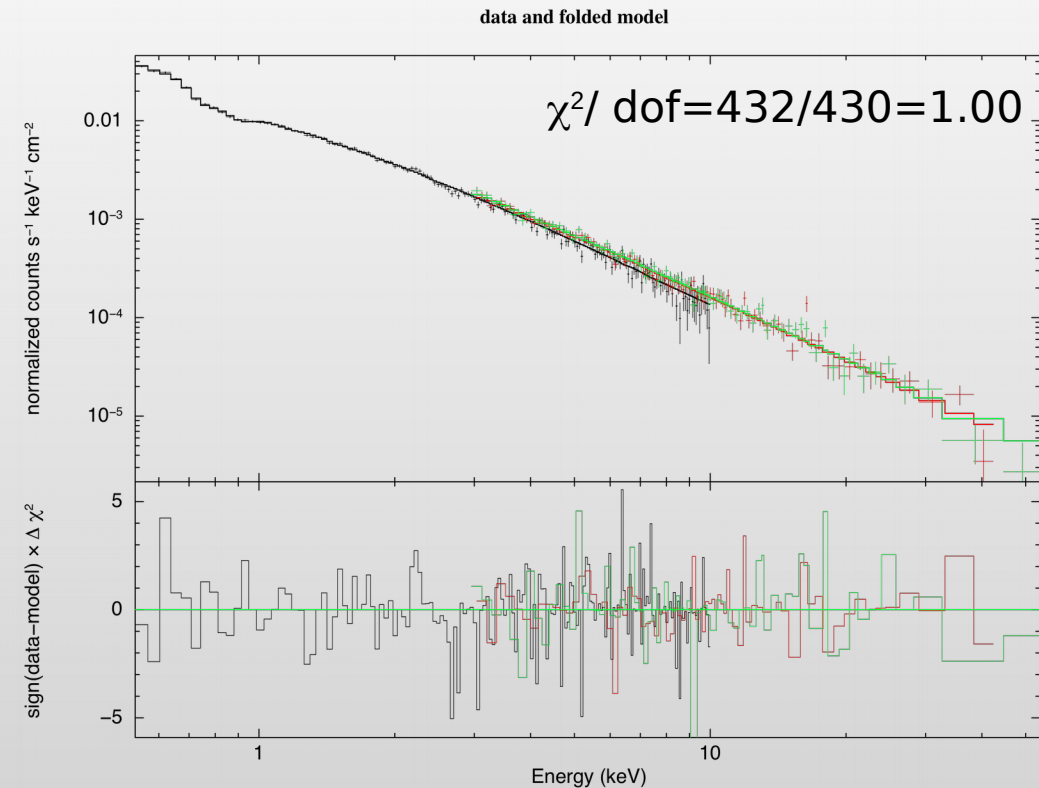


Backup



Difference between the highest flux spectrum (42.19 ± 0.07 cts/s) and a low flux one with constant HR (17.79 ± 0.04 cts/s)

A first fit with an absorbed power law leads to strong residuals, mainly due to the warm absorbing structure



$$N_{\text{H1}} = (9.8 \pm 2.5) \times 10^{21} \text{ cm}^{-2}$$

$$\log \xi_1 = 2.0 \pm 0.1$$

$$\Gamma = 2.16 \pm 0.03$$

$$N_{\text{H2}} = (2.1 \pm 1.9) \times 10^{21} \text{ cm}^{-2}$$

$$\log \xi_2 = 1.4 \pm 0.2$$

$$\log N_{\text{Fe}} = 17.2 \pm 0.3$$